Vertical bonding distances and interfacial band structure of PTCDA on a Sn-Ag surface alloy

Johannes Knippertz,[1,*] Leah L. Kelly,[1] Markus Franke,[2,3] Christian Kumpf,[2,3] Mirko Cinchetti,[4] Martin Aeschlimann,[1] and Benjamin Stadtmüller[1,5]

[1]*Department of Physics and Research Center OPTIMAS, University of Kaiserslautern, Erwin-Schroedinger-Strasse 46, 67663 Kaiserslautern, Germany*

[2]*Peter Grünberg Institut (PGI-3), Forschungszentrum Jülich, 52425 Jülich, Germany*

[3]*Jülich-Aachen Research Alliance (JARA)–Fundamentals of Future Information Technology, 52425 Jülich, Germany*

[4]*Experimentelle Physik VI, Technische Universität Dortmund, 44221 Dortmund, Germany*

[5]*Graduate School of Excellence Materials Science in Mainz, Erwin Schroedinger Strasse 46, 67663 Kaiserslautern, Germany*

(Received 24 January 2020; revised 7 July 2020; accepted 6 August 2020; published 28 August 2020)

Molecular materials enable a vast variety of functionalities for novel electronic and spintronic devices. The unique possibility to alter organic molecules or metallic substrates offers the opportunity to optimize interfacial properties for almost any desired field of application. For this reason, we extend the successful approach to control metal-organic interfaces by surface alloying. We present a comprehensive characterization of the structural and electronic properties of the interface formed between the prototypical molecule PTCDA and a Sn-Ag surface alloy grown on an Ag(111) single crystal surface. We monitor the changes of adsorption height of the surface alloy atoms and electronic valence band structure upon adsorption of one layer of PTCDA using the normal incidence x-ray standing wave technique in combination with momentum-resolved photoelectron spectroscopy. We find that the vertical buckling and the surface band structure of the $SnAg_2$ surface alloy is not altered by the adsorption of one layer of PTCDA, in contrast to our recent study of PTCDA on a $PbAg_2$ surface alloy [B. Stadtmüller *et al.*, Phys. Rev. Lett. **117**, 096805 (2016)]. In addition, the vertical adsorption geometry of PTCDA and the interfacial energy level alignment indicate the absence of any chemical interaction between the molecule and the surface alloy. We attribute the different interactions at these PTCDA/surface alloy interfaces to the presence or absence of local σ-bonds between the PTCDA oxygen atoms and the surface atoms. Combining our findings with results from literature, we are able to propose an empiric rule for engineering the surface band structure of alloys by adsorption of organic molecules.

DOI: 10.1103/PhysRevB.102.075447

I. INTRODUCTION

In the fast growing field of organic electronics and spintronics, it was soon realized that the device-relevant properties of molecular assemblies on surfaces are determined by the intrinsic properties of the active molecular materials and the metallic substrates as well as by the phenomena occurring at the interfaces between both materials. While the most important intrinsic properties of molecular materials and metallic substrates are rather well understood today [1–6] (and references therein), the interfacial properties of metal-organic (hybrid) interfaces are still subject of intense investigations. This is mainly due to the large complexity of such interfaces, which is rooted in the delicate interplay between different types of molecule-surface and intermolecular interactions that can occur in such systems [6–8]. These interactions can result in a severe modification of both sides of the metal-organic interfaces, and in selected cases, in the emergence of exotic phenomena such as adsorption-induced magnetic order in otherwise diamagnetic surfaces [9].

For the metal side, the molecule-surface interaction can lead to a depopulation and therefore a shift or a suppression of the metallic surface states upon the adsorption of organic molecules [10–12]. On the molecular side, weak chemisorption of organic complexes on metallic surfaces can result in a charge redistribution across the interface typically coinciding with charge transfer from the surface bands into the former lowest unoccupied molecular orbital (LUMO) [13–15]. Thereby, the amount of charge transfer into the molecular layer crucially depends in the interfacial interaction strength [16,17]. For an even stronger chemical interaction between molecules and surfaces, new states can be formed due to the hybridization between molecular and metallic states. These so-called hybrid interface states are most frequently observed on highly reactive transition metal surfaces [18–20].

In the past, different approaches have been demonstrated to control the interfacial properties of metal-organic interfaces, for instance by the formation of heteromolecular structures [21,22], metal-organic networks [23,24], or by alkali-metal doping [25–29]. In this work, we follow an alternative route and continue our recent approach of controlling the interaction strength across metal-organic interfaces by surface alloying. A surface alloy is a low-dimensional material that is ideally suited for tailoring hybrid interfaces since its geometric and

*jseidel@rhrk.uni-kl.de

electronic properties as well as the surface reactivity of noble metal surfaces can be tuned by the right choice of the alloy atom. For instance, the vertical buckling of the surface atoms can be varied from 0.10 Å to 0.65 Å by selecting the appropriate alloy atom [30]. Crucially, the hybrid surface states of these alloys reveal a Rashba-type spin splitting which hence allows to manipulate the spin degree of freedom of surface alloys by altering the chemical properties of the alloy atoms as well as the strength of their atomic spin-orbit coupling [31–34]. Moreover, ferromagnetic order has been recently observed in surface alloys formed between noble metal host materials and rare earth alloying atoms by Ormaza *et al.* [35], making this class of 2*d* materials even more interesting for spintronic applications. To further explore the adsorption-induced tuneablity of surface alloys, we investigate the interfacial properties of the prototypical molecule 3-, 4-, 9-, and 10-perylenetracarboxylic dianhydride (PTCDA, $C_{24}H_8O_6$) on a $SnAg_2$ surface alloy using a combination of surface sensitive techniques such as core-level spectroscopy, normal-incidence x-ray standing waves, and momentum-resolved photoemission. We find a significant reduction of the interaction strength between the PTCDA molecules and the Ag(111) surface by the implantation of Sn atoms in the first Ag layer. This reduction is reflected both by the vertical distance between the surface atoms and the PTCDA molecules as well as by the lack of charge transfer between the surface and the LUMO of PTCDA. It is also responsible for the persistence of the surface band structure of the $SnAg_2$ surface alloy after the adsorption of PTCDA. This adsorption-induced passivation of the surface alloy clearly differs from the adsorption-induced modification of the surface band structure of the similar $PbAg_2$ surface alloy by the formation of σ-like molecule surface bonds [36]. However, these surprisingly different behaviors allows us to propose an empirical design rule for engineering the surface band structure of alloys by the adsorption of molecular complexes.

II. EXPERIMENTAL DETAILS

A. Sample preparation

All experiments were carried out under ultra-high vacuum (UHV) conditions at a base pressure of 5×10^{-10} mbar at room temperature. The Ag(111) single crystals were cleaned by multiple cycles of Ar-Ion sputtering at various ion energies of 0.5 to 2.0 keV, $I_{\text{drain}} = 8\,\mu$A and subsequent sample annealing for 20 min up to 730 K. The (chemical) cleanness of the sample surface was confirmed by the existence and linewidth of the Shockley surface state and by core level spectroscopy (XPS). In particular, no signal of Sn was observed after the cleaning cycles indicating a neglecting diffusion of Sn atoms into the bulk of the Ag(111) crystal upon sample annealing. The $SnAg_2$ surface alloy was prepared by depositing Sn atoms onto the clean Ag(111) surface at elevated sample temperatures ($T = 550$ K) using a homebuilt thermal Sn evaporator. After deposition, the sample was kept at elevated temperatures for at least 30 min to increase the homogenity of the surface alloy. The sample coverage was confirmed after deposition by XPS via comparison of the areas of Sn 3*d* peaks to reference data. The organic molecules were subsequently deposited from a commercial Kentax evaporator with an evaporation temperature of $T = 570$ K. The molecular film of PTCDA was deposited with a rate of approximately one monolayer per 10 min. The sample coverage was confirmed by comparing the intensity of the C 1*s* core level signal of PTCDA on $SnAg_2$ with the one of PTCDA/Ag(111). We chose this reference system since a PTCDA layer with a coverage of precisely 1.0 ML can be prepared by thermal desorption of a multilayer film [37].

B. Experimental methods

The momentum-resolved photoemission data were obtained by momentum microscopy at the University of Kaiserslautern [38,39]. The core level and normal incidence standing waves experiments were performed at beamline I09 of the Diamond Light Source (DLS) in Didcot, UK [40]. This end station is equipped with a hemispherical electron analyzer (Scienta EW4000 HAXPES), which is mounted perpendicular to the direction of the incoming photon beam. This analyzer has an angular acceptance of $\pm30^\circ$ and an energy resolution of 150 meV using the analyzer settings of our experiments ($E_{\text{pass}} = 100$ eV, $d_{\text{slit}} = 0.5$ mm). The NIXSW method is a powerful tool to investigate the adsorption height of chemically inequivalent atoms above a single crystalline surface with a precision of $\Delta z \leqslant 0.04$ Å. While a detailed description of the method can be found elsewhere [41–43], we just give a short summary of the basic principle.

For photon energies fulfilling the Bragg condition for a specific reflection $H = (hkl) = k_H - k_0$, a standing wave field is formed above the single crystal due to the interference between the incoming and reflected x-ray wave field. Scanning the photon energy through the Bragg condition, one observes a phase shift of the relative complex amplitudes between the incoming and the reflected wave by π. This phase shift results in a displacement of the standing wave field by half a lattice spacing $d_{(hkl)}$ in the direction perpendicular to the Bragg planes. This shift of the standing wave field changes the photon density at any specific position z above the single crystal surface as a function of the photon energy. If an atom is located at a position z above the single crystal surface, its XPS yield changes depending on the position of the standing wave field, e.g., the used photon energy. The experimentally observed yield curve $I(E)$ can be described by

$$I(E) = 1 + S_R R(E) + 2|S_I|\sqrt{R(E)} \cdot F^H \cos\left[\nu(E) - 2\pi P^H + \Psi\right], \quad (1)$$

where $R(E)$ is the x-ray reflectivity of the Bragg reflection with its complex amplitude $\sqrt{R(E)}$ and phase $\nu(E)$. S_R, $|S_I|$, and Ψ are correction parameters for nondipolar contributions to the photoemission yield [44–47] for emission from an *s*-state. The fitting parameters of the NIXSW analysis are the coherent fraction F^H and coherent position P^H. The coherent position P^H can be interpreted as an average height of the chemical species with respect to the Bragg planes: $z = d(h\,k\,l)\cdot(P^H + n)$, $n = 0, 1, 2, \ldots$, where n is the number of Bragg planes located between the surface plane and the average position of the species. The coherent fraction F^H is a parameter quantifying the vertical order of this atomic species.

In ideal cases, perfect vertical order corresponds to a coherent fraction $F^H = 1$, while a homogeneous distribution of adsorbates between two Bragg planes would lead to a coherent fraction $F^H = 0$. For single layers of molecular adsorbates on surfaces, coherent fractions of carbon, nitrogen or oxygen atoms are typically in the range of $F^H = 0.8$ even for highly ordered molecular layers [14]. This reduction of F^H can be attributed to molecular vibrations and small structural defects in the molecular film which can have a significant influence on the vertical order of carbon, nitrogen and oxygen atoms due to the typically large number of these atomic species in the molecular complexes.

III. EXPERIMENTAL RESULTS

A. Lateral structure

We now turn to the discussion of the experimental results and start with the lateral order of the PTCDA/$SnAg_2$ interface. The bare $SnAg_2$ surface alloy has already been studied recently by Osiecki *et al.* [48]. Briefly, in unison with other surface alloys on fcc(111) noble metal surfaces [30,32–34], the $SnAg_2$ alloy exhibits a homogeneous $(\sqrt{3}\times\sqrt{3})R30^\circ$ superstructure that is formed by replacing each third Ag surface atom by Sn. The corresponding low-energy electron diffraction (LEED) pattern of this superstructure is shown in Fig. 1(a). The corresponding structural model of the $SnAg_2$ surface alloy is shown in Fig. 1(c) with Sn atoms shown in cyan and Ag atoms shown in grey.

After the adsorption of one monolayer of PTCDA onto the clean $SnAg_2$ surface alloy, we observe a set of new, well-defined spots in LEED [Fig. 1(b)] indicating the formation of a long-range ordered molecular overlayer. Interestingly, the LEED pattern of the PTCDA/$SnAg_2$ interface exhibits the typical arrangement of diffraction spots in double triangular structures known for PTCDA monolayer films on bare fcc(111) noble metal surfaces. For a quantitative analysis of the LEED data, we simulated diffraction patterns for various structures and found the best agreement between the LEED data and the simulations for the superstructure with the matrix $\left(\begin{smallmatrix}7 & 1\\ 2 & 5\end{smallmatrix}\right)$ with respect to the Ag(111) surface unit cell. This matrix is identical to one for the PTCDA monolayer structure on Ag(111) [37,49] and indicates that the overlayer is commensurate with the silver surface lattice. Consequently, it is also commensurate with the $(\sqrt{3}\times\sqrt{3})R30^\circ$ lattice of $SnAg_2$ alloy in higher order:

$$3\cdot\begin{pmatrix}\vec{A}\\ \vec{B}\end{pmatrix}_{\mathrm{PTCDA}} = \begin{pmatrix}8 & -5\\ 7 & 8\end{pmatrix}\cdot\begin{pmatrix}\vec{A}\\ \vec{B}\end{pmatrix}_{\mathrm{SnAg_2}} = \begin{pmatrix}21 & 3\\ 6 & 15\end{pmatrix}\cdot\begin{pmatrix}\vec{A}\\ \vec{B}\end{pmatrix}_{\mathrm{Ag}}.$$

The molecular structure of the PTCDA monolayer film on the $SnAg_2$ surface alloy is illustrated by our structural model in Fig. 1(c). This model is adopted from the one for the monolayer structure of PTCDA adsorbed on Ag(111) and exhibits two PTCDA molecules per unit cell arranged in a herringbone pattern, see unit cell marked in white. The much larger unit cell that is commensurate with the $SnAg_2$ surface alloy is marked in black. It exhibits 18 PTCDA molecule in

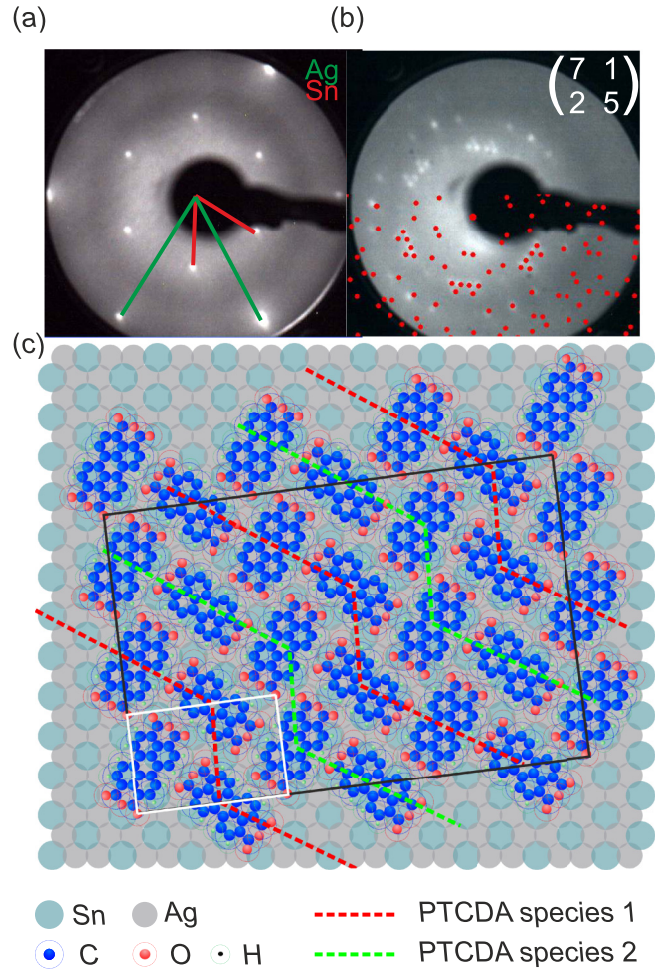

FIG. 1. (a) LEED image recorded for $SnAg_2$ surface alloy formed on Ag(111) ($E_{\mathrm{kin}} = 76$ eV). The unit cell basis vectors of the substrate in momentum space are indicated in green, the one of the $(\sqrt{3}\times\sqrt{3})R30^\circ$ superstructure in red. (b) LEED image for a monolayer of PTCDA on $SnAg_2$ surface alloy ($E_{\mathrm{kin}} = 14$ eV). The bottom half of the LEED image is superimposed with simulated diffraction spots of the superstructure matrix of PTCDA/Ag(111): $\left(\begin{smallmatrix}7 & 1\\ 2 & 5\end{smallmatrix}\right)$. (c) structural model of the PTCDA monolayer film on the $SnAg_2$. The small unit cell with two PTCDA molecules is marked in white, the larger unit cell that is commensurate with the $SnAg_2$ superstructure in black.

two azimuthal orientations with respect to the surface lattices. A closer inspection of the local adsorption configuration of the PTCDA/$SnAg_2$ superstructure reveals that half of the PTCDA molecules can be associated with an adsorption site with four Sn atoms located underneath the carbon backbone (PTCDA species 1, indicated by a red dashed line) while the other molecules can be associated with an adsorption site with five Sn atoms underneath the carbon backbone (PTCDA species 2, indicated by a green dashed line). Interestingly, PTCDA molecules with both azimuthal orientations can be observed on both adsorption sites associated either with four or five Sn atoms resulting in at least four different adsorption sites of PTCDA on the $SnAg_2$ surface alloy. An even more detailed inspection of the adsorptions sites indicates a strong variation of the lateral distribution of Sn atoms below PTCDA

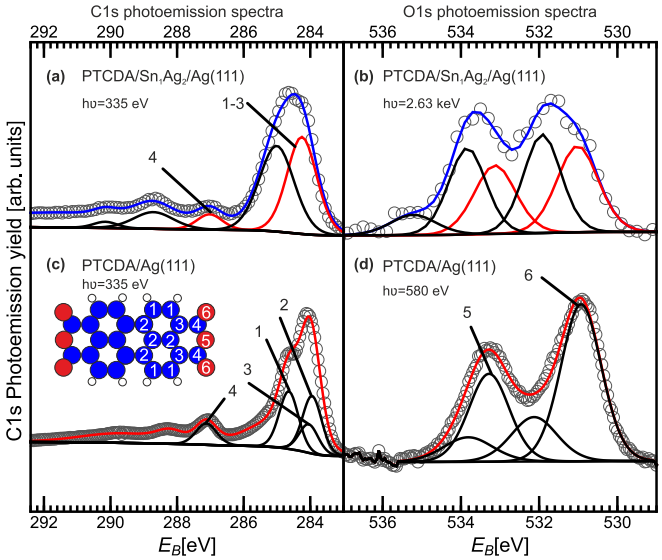

FIG. 2. The C 1*s* (left) and O 1*s* (right) core level spectra for the monolayer structure of PTCDA on (a), (b) the $SnAg_2$ surface alloy, and (c), (d) the clean Ag(111) surface.

species 1 which is absent for PTCDA species 2. Finally, the existence of multiple adsorption sites together with the higher-order commensurability between the PTCDA and the $SnAg_2$ surface alloy already suggests a rather weak influence of the $SnAg_2$ surface on the adsorption geometry of the PTCDA molecules of the monolayer film.

B. Core level spectroscopy

To characterize the electronic structure of the interface, we performed core level spectroscopy studies using both the soft and hard x-ray branches of the I09 beamline. In Figs. 2(a) and 2(b) we show C 1*s* and O 1*s* core level spectra for a layer of PTCDA adsorbed on $SnAg_2$. For comparison, we also included the corresponding spectra for PTCDA on the bare Ag(111) surface [Figs. 2(c) and 2(d)]. The red and black curves in Figs. 2(a) and 2(b) correspond to the fitting models for the PTCDA species $PTCDA_1$ and $PTCDA_2$.

The C 1s emission line of PTCDA on Ag(111) consists of the four contributions of four chemically inequivalent carbon atoms. These chemically different carbon atoms are shown in the inset of Fig. 2(c) and are labeled (1) for C-H, (2) for C-C, (3) for C-C-O, and (4) for C-O [15,51]. While the carbon atoms (1) to (3) are responsible for the C 1s main line at $E_B = 284.0$ eV, the C-O carbon atoms (4) lead to a well-separated feature at larger binding energies. Turning to the C 1*s* core level spectrum of PTCDA on the $SnAg_2$ surface alloy, we find an intense main line with asymmetric lineshape and at least two well-separated peaks at larger binding energies. The existence of two well-separated peaks at binding energies larger than the main line is attributed to the C-O carbon signals of two chemical inequivalent types of PTCDA molecules on the surface alloy. To further analyze the C 1*s* linshape we developed an effective fitting model based on our previous core level analysis of PTCDA on a similar surface alloy [36,50]. The individual components of our fitting model are shown as red and black curves in Fig. 2(a) and their binding energies are summarized in Table I. The C 1*s* line shape of each PTCDA species is described by a main line combining the emission of the carbon atoms (1) to (3) and a separated peak for the C-O (4) carbon atoms. As we will discuss in the NIXSW section below, we can identify the main line of the species $PTCDA_1$ [red curves in Fig. 2(a)] at identical binding energy as known for PTCDA on the bare Ag(111) surface while the one of the species $PTCDA_2$ is shifted 0.76 eV to larger binding energies. The magnitude of this shift is comparable to the energy difference between the main lines of a PTCDA monolayer and multilayer film on Ag(111) [51].

TABLE I. XPS peak positions as shown in Fig. 2.

Species	C $1s_{main}$ [eV]	C $1s_{C\text{-}O}$ [eV]	O $1s_a$ [eV]	O $1s_c$ [eV]
1	280.3	283.1	532.9	530.8
2	281.1	284.8	533.6	531.7

The excellent quality of the fit does not only confirm the existence of two chemically inequivalent PTCDA molecules on the $SnAg_2$ surface alloy but also allows us to estimate a balanced ratio between both PTCDA species on the surface. This stoichiometry is almost 1:1(precisely 52:48) and therefore consistent with our structural model.

The analysis of the O 1*s* core level data leads to a very similar conclusion. The lineshape of the O 1*s* core level emission of $PTCDA/SnAg_2$ reveals a similar double peak structure with an additional shoulder on its low binding energy side ($E_B = 535.5$ eV), see in Fig. 2(d). This last case is clearly absent for PTCDA on the bare Ag(111) surface as illustrated by the reference spectrum in Fig. 2(d). In analogy to the C 1*s* core level spectrum, we analyzed the O 1*s* lineshape with a superposition of two core level signatures of chemically inequivalent PTCDA molecules. The fit envelope is depicted as solid blue line, the corresponding contributions of both types of PTCDA molecules as red and black solid lines. For both types of molecules, we considered two chemically inequivalent oxygen species, namely the carboxylic (6) and the anhydride (5) oxygen species of PTCDA [52]. The best fit was obtained for the model shown in Fig. 2(b). Analyzing the integrated intensity of the O 1*s* fitting curves yields again an almost balanced ratio of the core level signatures of both types of PTCDA of 52:48. This is in exact agreement with our findings for the C 1*s* core level analysis.

C. Vertical adsorption configuration

The existence of two characteristic PTCDA adsorption sites with different chemical environment can also have a profound influence on the bonding of both PTCDA species on the $SnAg_2$ surface alloy. The latter can be obtained by investigating the vertical adsorption configuration and the molecule-surface bonding distance of the $PTCDA/SnAg_2$ interface using the NIXSW technique. For the NIXSW analysis, we used the core level models for the C 1*s* and O 1*s* emission discussed above. In the fitting procedure, we constrained the relative intensities of all chemically different C and O species, separately for each of the two types of PTCDA molecules. Furthermore, the binding energy positions and FWHM of all

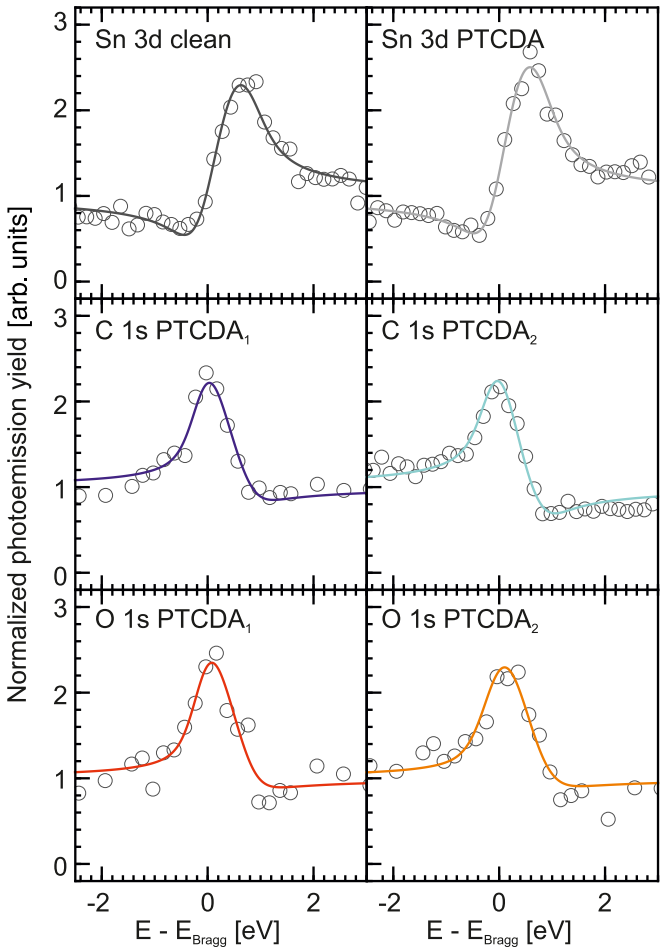

FIG. 3. Exemplary partial yield curves of individual NIXSW scans for the Sn atoms prior or after the adsorption of PTCDA, as well as of the carbon and oxygen atoms of both types of PTCDA molecules on the $SnAg_2$ surface alloy.

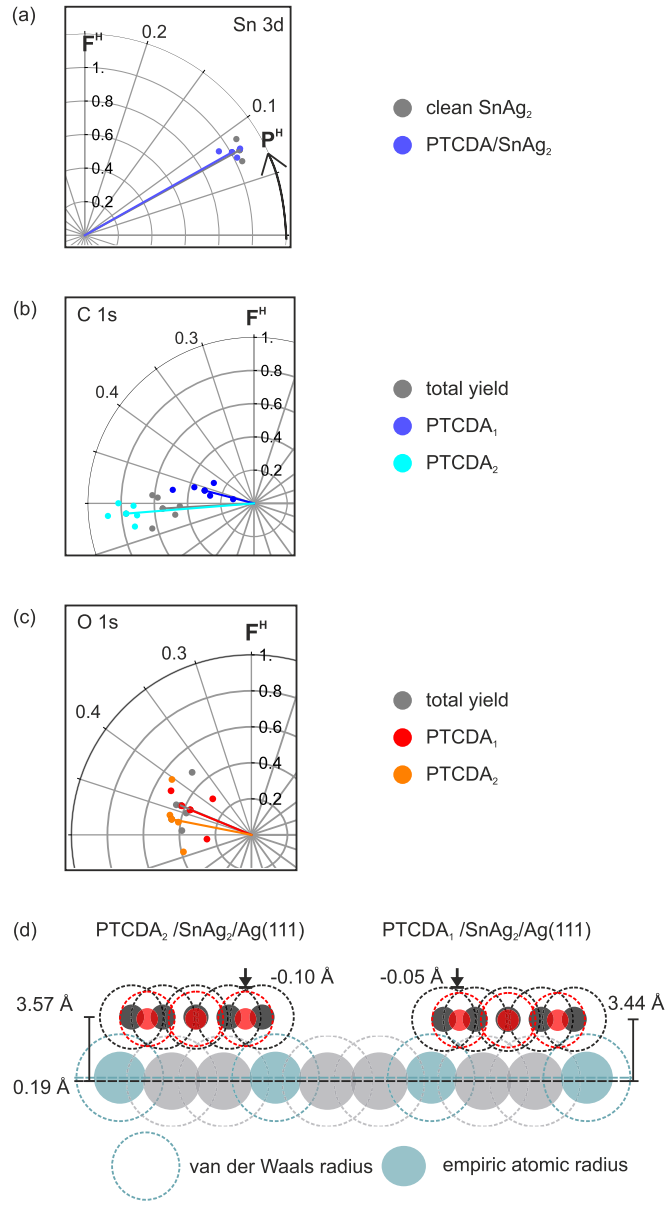

FIG. 4. (a) Argand diagram illustrating the NIXSW results for the Sn species of the $SnAg_2$ surface alloy, prior and after the adsorption of a monolayer of PTCDA. (b), (c) Argand diagram for the results of the C 1*s* and O 1*s* core levels, respectively, of a PTCDA monolayer on $SnAg_2$. (d) Real-scale vertical adsorption geometry model for PTCDA adsorbed on Sn_1Ag_2 surface alloy.

Gaussian peaks were kept constant in the fitting. For each of the two chemically inequivalent PTCDA molecules this results in two free fitting parameters for the adsorption heights, one for the (average height of all) carbon atoms and one for the (average height of all) oxygen atoms. While this severely reduces the structural information obtained in the NIXSW experiment, it was necessary to obtain reliable fitting results. The photoemission yield of the Sn 3*d* core level was only extracted from a very narrow angular range at an emission angle of 90° with respect to the surface normal. Under this angle, the nondipolar contributions to the photoemission yield are minimal. This is the only way to obtain reliable NIXSW fitting results when photoelectrons from 3*d* states are used for the NIXSW measurements since non-dipolar corrections are only possible for emission from *s*-states. For all atomic species, the core level data were analyzed with the commercial software CASAXPS. Uncertainties of the photoemission yield curve were estimated by the implemented Monte Carlo error analysis [53,54]. They are usually in the range of 10% and are omitted in the plots for better visibility.

We present exemplary yield curves for all atomic species in Fig. 3. The yield curves are analyzed with the NIXSW analysis software TORICELLI [55,56] resulting in the fitting parameters coherent position P^H and coherent fraction F^H [see Eq. (1)]. For each species, several scans at different sample positions were recorded and analyzed individually. The fitting results are presented in the Argand diagrams in Fig. 4: the length of each polar vector represents the coherent fraction, the polar angle with respect to the *x*-axis the coherent positions. The results for the Sn, C, and O species are shown in Figs. 4(a), 4(b), and 4(c), respectively, as colored circles for each individual NIXSW scan, and as arrow of identical color for the corresponding average values. The experimental uncertainty of the fitting parameters and the adsorption height

TABLE II. NIXSW fitting results and corresponding adsorption heights of all analyzed species of the PTCDA/$SnAg_2$ interface. For comparison, adsorption heights for PTCDA on the Ag(111) surface are included [50,52]. We used nondipolar correction parameters of $\gamma = 1.06219$ (0.97470) for the C 1*s* (O 1*s*) emission lines. The experimental geometry is given by the Bragg angle of $\theta = 86.5^\circ$ (3.5° off normal incidence) and by $\phi = 75^\circ$ (photoelectron emission angle relative to incident beam) [47,55]. For the analysis of the Sn 3*d* core level, we only considered the photoemission yield in a narrow angle range close to an emission angle of 90° to minimize the influence of nondipolar contributions to the photoemission signal.

	F^H	P^H	D^H_{SnAg} [Å]	D^H_{Ag} [Å]
Sn $3d_{alloy}$	1.05 ± 0.05	0.08 ± 0.01	0.19 ± 0.02	–
Sn $3d_{PTCDA}$	1.01 ± 0.03	0.08 ± 0.03	0.19 ± 0.008	–
C $1s_{PTCDA,1}$	0.27 ± 0.08	0.46 ± 0.01	3.44 ± 0.03	2.86 ± 0.01
C $1s_{PTCDA,2}$	0.69 ± 0.05	0.51 ± 0.01	3.57 ± 0.02	2.86 ± 0.01
O $1s_{PTCDA,1}$	0.33 ± 0.07	0.43 ± 0.03	3.39 ± 0.05	2.77 ± 0.05
O $1s_{PTCDA,2}$	0.41 ± 0.04	0.46 ± 0.03	3.45 ± 0.07	2.77 ± 0.05

of each species are calculated by the standard deviation of the individual fitting results. These averaged fitting parameters for P^H and F^H are summarized in Table II together with the corresponding adsorption heights. As a reference we included the adsorption heights of all atomic species for PTCDA on Ag(111) [52].

For the bare $SnAg_2$ surface alloy (before adsorption of PTCDA), we find a coherent fraction of $F^{\mathrm{H}}_{\mathrm{Sn}} = 1.05 \pm 0.05$ and a coherent position of $P^{\mathrm{H}}_{\mathrm{Sn}} = 0.08 \pm 0.01$. The experimental uncertainties are rather small, as reflected by the marginal scattering of the fitting results of the individual NIXSW scans in the Argand diagram in Fig. 4(a). The corresponding adsorption height of Sn is 0.19 ± 0.02 Å with respect to the surface plane of the Ag atoms, i.e., the Sn atoms show a small vertical relaxation from the surface layer towards the vacuum. This relaxation is very uniform, as reflected by the large coherent fraction F^H which is just within the physically meaningful limit of $F^H \leqslant 1$. We attribute this high value to an overestimation of F^H caused by nondipolar contributions of the Sn 3*d* photoemission yield which cannot be perfectly suppressed by our experimental geometry. However, nondipolar contribution can typically only alter F^H by ≈10% and hence do not significantly alter the interpretation of our findings. Interestingly, our experimental findings cannot confirm recent theoretical predictions for a small vertical inwards relaxation ($\Delta z = -0.04$ Å) of the Sn atoms of a $SnAg_2$ surface alloy towards the Ag bulk [48]. Moreover, the vertical relaxation of the Sn atoms from the Ag surface plane is comparable to the relaxation of Sb, but significantly smaller than the relaxation of other surface alloy atoms such as Bi or Pb [30]. We attribute this difference to the smaller atomic size of Sn or Sb compared to Bi and Pb.

The adsorption of one layer of PTCDA on the $SnAg_2$ surface alloy does not change the vertical positon of the Sn atoms (within experimental uncertainties), as we find almost identical coherent positions and coherent fractions before and after the adsorption of PTCDA. This is clearly different compared to our recent study of PTCDA on the $PbAg_2$ surface alloy where we observed an additional vertical relaxation of the Pb surface alloy atoms of $\Delta z = 0.08 \pm 0.01$ Å upon the adsorption of PTCDA [50]. The NIXSW fitting results for the carbon and oxygen atoms are shown in the Argand diagram Figs. 4(b) and 4(c). The scattering of the fitting results for both elements is significantly larger than for the Sn surface alloy atoms resulting in larger experimental uncertainties of the vertical positions of both types of PTCDA molecules. In addition, the coherent fractions of the carbon and oxygen atoms of both PTCDA molecules are clearly different. The coherent fractions of $F^{\mathrm{H}}_{\mathrm{C}1s} = 0.69 \pm 0.05$ and $F^{\mathrm{H}}_{\mathrm{O}1s} = 0.41 \pm 0.04$ of $PTCDA_2$ are comparable to the coherent fractions obtained for flat lying PTCDA molecules on other noble metal surfaces. Note that the coherent fraction of oxygen is expected to be smaller than for carbon, if the two species (carboxylic and anhydride oxygen) are not evaluated separately since slightly different adsorption heights were reported for the different oxygen species for adsorption on noble metal surfaces [59]. However, the corresponding fractions of $PTCDA_1$ of $F^{\mathrm{H}}_{\mathrm{C}1s} = 0.27 \pm 0.08$ and $F^{\mathrm{H}}_{\mathrm{O}1s} = 0.33 \pm 0.07$ are significantly lower than typical values for flat lying molecules. One possible reason for such low coherent fractions of $PTCDA_2$ might be a not complete separation of the core level intensities in the XPS fitting model. In such a case the yield attributed to $PTCDA_1$ would also contain intensity of $PTCDA_2$ and hence a too small coherent fraction would be found when both molecules exhibit different adsorption. To estimate the effect of such a unprecise analysis we additionally employed a vector component analysis. In the Argand diagram, each NIXSW fitting result can be represented by a vector $\mathbf{Z}(F^H, P^H) = F^H \cdot e^{i2\pi P^H}$. For PTCDA/$SnAg_2$, the NIXSW fitting results of the total yield signal $\bar{Z}(F^H_{TY}, P^H_{TY})$ (background-corrected intensity of the entire core level spectrum) contain two contributions, one form $PTCDA_1$ molecules $[\mathbf{Z}(F^H_{P1}, P^H_{P1})]$ and one form $PTCDA_2$ molecules $[\mathbf{Z}(F^H_{P2}, P^H_{P2})]$. The total yield vector $\mathbf{Z}(F^H_{TY}, P^H_{TY})$ can hence be obtained by

$$\mathbf{Z}\left(F^H_{TY}, P^H_{TY}\right) = a \cdot \mathbf{Z}\left(F^H_{P1}, P^H_{P1}\right) + (1-a) \cdot \mathbf{Z}\left(F^H_{P2}, P^H_{P2}\right), \qquad (2)$$

where a is the relative contribution of $PTCDA_1$ to the total yield signal. In a first step, we employ the vector component analysis to estimate the coherent positions (i.e., the adsorption heights) of both PTCDA molecules from the NIXSW fitting results of the total carbon yield. The latter are shown as grey points in the Argand diagram in Fig. 4(b) and their average values are included in Table II. The relative contribution a is determined by the stoichiometric ratio of both molecular species of 52:48 and we assume an identical coherent fraction for both PTCDA species of $F^H_{P1/2} = 0.75$. This value is typically observed for PTCDA molecules in a flat adsorption geometry on noble metal surfaces [6]. We find coherent positions P^H of 0.38 and 0.63 for the two PTCDA species corresponding to a vertical distance between them of $\Delta z = 0.59$ Å. This value appears to be too high for two molecules lying in one layer, as demonstrated by other reference systems with two structurally inequivalent molecules on surfaces [36]. More realistic vertical distances can only be obtained when reducing the coherent fraction of $PTCDA_1$ below 0.4. Similar findings were also obtained for the vector component analysis of the O 1*s* data. Therefore, the small coherent fraction of $PTCDA_1$

cannot be explained merely by a not completely correct fitting model for the XPS spectra. We believe that the weakly defined molecular adsorption site for this molecule (remember that the lateral distribution of Sn atoms located below the molecule was nonuniform for this molecular species, see discussion above) at least contributes significantly to the small coherent fractions we found. We propose that the lower vertical order of $PTCDA_1$ is directly linked to its adsorption site. As discussed earlier, one type of PTCDA molecules is located on ≈4 Sn atoms with local variations of the exact number of Sn atoms. The other type of PTCDA molecule is homogeniously located on five Sn molecules. We therefore propose that the low coherent fraction of $PTCDA_1$ is due to a local variation of the lateral distribution of Sn atoms below the carbon backbone and assign $PTCDA_1$ to the adsorption site associated with four Sn atoms (see red dotted line in Fig. 1). $PTCDA_2$ is consequently attributed to PTCDA molecules that are located above five Sn atoms of the surface alloy (see green dotted line in Fig. 1).

For a further discussion of the NIXSW results, the vertical adsorption geometry of both PTCDA molecules is shown in a true scale model in Fig. 4(d). The PTCDA molecules are drawn in a schematic side view along their long molecular axis. The colored circles indicate the (empiric) atomic radii while the dashed circles show the corresponding van der Waals radii [57]. This presentation provides a quantitative view onto the bonding distance between $PTCDA_2$ molecules and the $SnAg_2$ surface alloy. For $PTCDA_1$ molecules, this illustration is only an effective model of the interfacial adsorption configuration as it neglects the vertical disorder of $PTCDA_1$ molecules on the surface alloy. However, it will still allow us to qualitatively discuss the bonding type and strength of $PTCDA_1$ molecules with the $SnAg_2$ surface alloy. Upon adsorption on the $SnAg_2$ surface alloy, both types of PTCDA molecules exhibit almost no bending of the oxygen end groups towards the $SnAg_2$ surface alloy atoms. While the average adsorption position of the oxygen atoms of the anhydride endgroups is slightly below the carbon backbone ($\Delta z_{PTCDA,1} = -0.06 \pm 0.07$ Å, and $\Delta z_{PTCDA,2} = -0.12 \pm 0.07$ Å), this difference is barely significant within the experimental uncertainty. This observation is in clear contrast to the vertical adsorption geometry of PTCDA on $PbAg_2$ [50] surface alloy as well as on all low index silver surfaces [52,53,58]. On these surfaces, at least one chemical oxygen species (typically the carboxylic oxygen atoms) bends down towards the surface atoms. This vertical distortion of the PTCDA oxygen end groups is the geometric signature of the formation of local, σ-like bonds between the oxygen atoms of PTCDA and the surface. In contrast, the flat adsorption geometry of both inequivalent PTCDA molecules on the $SnAg_2$ surface alloy indicates the absence of such local bonds between the oxygen atoms and the Sn or Ag surface atoms. Such σ-bonds were identified as the microscopic origin of the vertical relaxation of the Pb atoms of the $PbAg_2$ surface alloy after the adsorption of PTCDA.

The carbon backbone of both PTCDA molecules is located at slightly different adsorption heights of $D^H_{PTCDA,1} = 3.44 \pm 0.03$ Å and $D^H_{PTCDA,2} = 3.57 \pm 0.02$ Å. A better representation of the distances between two atoms is given by the normalized bonding distance which is calculated by

$$d^N_{A-B} = \frac{d_{A-B}}{d^A_{VdW} + d^B_{VdW}}, \tag{3}$$

A and B label the different atomic species, d_{A-B} the distance between these atomic species, and $d^{A/B}_{VdW}$ the respective van der Waals radii. The normalized bonding distance is a very good indicator for the maximum interaction strength between two atoms A and B, i.e., it assumes an on-top adsorption site of the adsorbed atomic species on the substrate atom. While $d^N_{A-B} \approx 1$ represents very weak interaction (physisorption), smaller radii indicate partial overlap of the atomic van der Waals radii and thus stronger interaction. The results for the interfaces formed between PTCDA with $SnAg_2$, $PbAg_2$, and Ag(111) are summarized in Table III. We obtain higher normalized bonding distances in the $SnAg_2$ system compared to both $PbAg_2$ and Ag(111) for all atomic species.

TABLE III. Normalized bonding distances for PTCDA monolayer films on the $SnAg_2$, $PbAg_2$, and Ag(111) surfaces. Van der Waals radii were taken from [57]: $r_C = 1.77$ Å, $r_O = 1.50$ Å, $r_{Sn} = 2.42$ Å, $r_{Pb} = 2.54$ Å, and $r_{Ag} = 2.53$ Å.

	d^N_{SnAg} [%]	d^N_{PbAg} [%]	d^N_{Ag} [%]
C $1s_{PTCDA,1}$	78 ± 1.4	73 ± 1.2	68 ± 1.5
C $1s_{PTCDA,2}$	81 ± 1.2	77 ± 0.7	68 ± 1.5
O $1s_{carbox,1}$	82 ± 2.6	70 ± 0.7	68 ± 2.3
O $1s_{carbox,2}$	84 ± 2.6	77 ± 0.7	68 ± 2.3
O $1s_{anhy,1}$	82 ± 2.6	75 ± 2.5	76 ± 4.1
O $1s_{anhy,2}$	84 ± 2.6	80 ± 1.5	76 ± 4.1

Altogether, our investigation of the vertical adsorption geometry shows that surface alloying of the Ag(111) surface with Sn atoms suppresses the chemical interaction between PTCDA and the Ag(111) surface. In particular, we do not observe any vertical relaxation of the Sn surface alloy atoms which indicates the absence of local, σ-like bonds between the molecule and the Sn alloy atoms. In the following, we will explore the consequence of the physisorptive molecule-surface bonding for the surface band structure of the alloy and the interfacial energy level alignment at the interface.

D. Electronic valence band structure

The modification of the $SnAg_2$ surface band structure upon adsorption of PTCDA can be determined directly by momentum-resolved photoemission spectroscopy with vacuum-ultraviolet radiation. The band structure of the bare $SnAg_2$ is dominated by a hybrid surface state with a hole-like parabolic dispersion, which is located at the $\bar{\Gamma}$-point of the surface Brillouin zone [48]. In the momentum resolved photoemission data shown in Fig. 5(a), left side, this hybrid surface state appears as ring-like feature in the constant energy map (CE map) recorded at $E_B = 0.8$ eV (indicated by the green ring). Upon adsorption of PTCDA, no modification of the emission pattern or the band dispersion of this hybrid surface state is observed in the occupied valence band structure as exemplarily shown in the CE map in Fig. 5(a), right side. This clearly indicates that the electronic surface alloy structure of $SnAg_2$ is not significantly altered by adsorption of PTCDA.

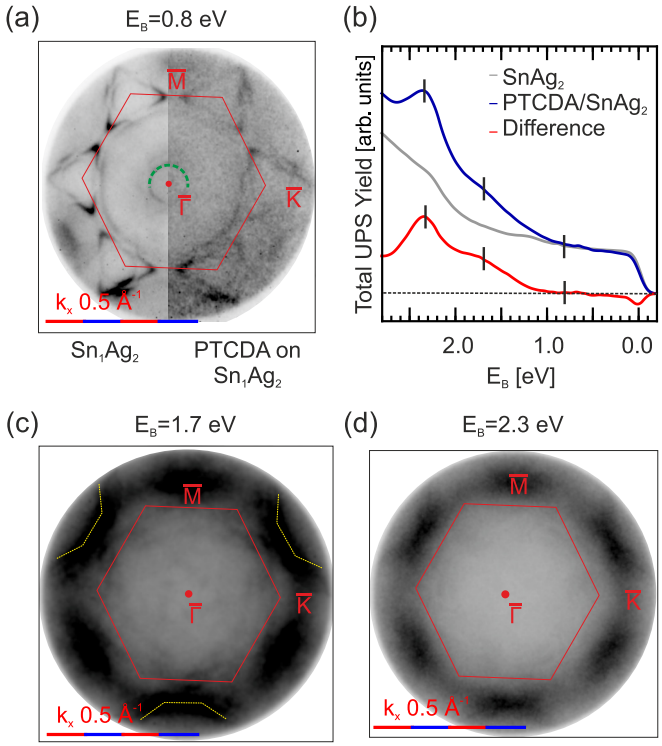

FIG. 5. (a) Constant energy map at 0.8 eV binding energy for the bare $SnAg_2$ surface alloy (left) and after adsorption of one layer of PTCDA (right). The hybrid interface state (indicated by a green ring) is not altered upon adsorption of PTCDA. (b) Total UPS yield of the electronic valence structure of PTCDA/$SnAg_2$ (blue), $SnAg_2$ (gray), and the difference signal (red). We observe no molecular features at E_F , but two at $E_B = 1.7$ eV and $E_B = 2.3$ eV. (c), (d) Symmetrized constant energy maps extracted at $E_B = 1.7$ eV and $E_B = 2.3$ eV , respectively, i.e., at the binding energy of the molecular features in the UPS spectrum.

To characterize the interfacial energy level alignment and to reveal a possible adsorption-induced charge redistribution across the interface, we recorded the total photoemission yield in the valence band structure, as shown in Fig. 5(b) as a solid blue line. As a reference, the total photoemission yield of the bare $SnAg_2$ surface alloy is shown as a gray solid line, and the difference signal in red.

Most importantly, the photoemission spectrum does not reveal any molecular feature in the vicinity of the Fermi edge, which would indicate an occupation of a LUMO-derived state. Such a state is usually observed for PTCDA on Ag(111) and was also found on the $PbAg_2$ surface alloy. This state becomes (at least) partly occupied due to an interfacial charge transfer from the surface into the molecule. It can be thus regarded as the spectroscopic signature of a partial chemical interaction between the molecule and the surface mediated by a delocalized π-bond at the interface [59]. The absence of such a state further supports our previous conclusion of a mere physisorption of PTCDA on the $SnAg_2$ surface alloy.

The two photoemission features at $E_B = 1.7$ eV and $E_B = 2.3$ eV can be assigned to the highest-occupied molecular orbitals (HOMO) of the two chemically inequivalent PTCDA molecules. This assignment is based on the CE maps of both HOMO features in Figs. 5(c) and 5(d). Both CE maps reveal the characteristic emission pattern of the PTCDA HOMO on a threefold symmetric fcc(111) surface with six well-defined maxima located on a ring with $r \approx 1.7$ Å^{-1} in momentum space [60]. The feature at $E_B = 1.7$ eV corresponding to the HOMO of $PTCDA_1$ is slightly less well defined due to an overall lower intensity. For this reason, the *sp*-bands of the surface alloy still contribute to the intensity distribution in this constant energy map. These *sp*-bands are highlighted by a dashed yellow line and lead to a distortion of the expected elliptical shapes of the molecular emission pattern due to the superposition of the molecular orbital feature and substrate bands. The significant difference in the binding energies of the HOMOs of both types of PTCDA molecules is mainly due to a shift of the HOMO of $PTCDA_1$ with respect to its binding energy in the gas phase. This indicates a stronger molecule-surface interaction of $PTCDA_1$ compared to $PTCDA_2$ and is in agreement with the NIXSW results showing a smaller adsorption height for this molecule.

IV. DISCUSSION

Our comprehensive investigation of the structural and electronic properties of PTCDA on the $SnAg_2$ surface alloy has revealed clear signatures of a nonchemical interaction between PTCDA and the underlying surface alloy. We find a nondistorted adsorption geometry of PTCDA as well as the absence of any charge transfer across the interface. In addition, the vertical buckling of the Sn surface alloy atoms and the surface band structure of the $SnAg_2$ surface alloy are fully preserved after the adsorption of PTCDA. Our findings for PTCDA/$SnAg_2$ are hence qualitatively similar to those of CuPc on the $PbAg_2$ surface alloy, a molecular adsorbate system that only forms delocalized π-bonds with surfaces. In particular, the interfacial properties of PTCDA/$SnAg_2$ are significantly different compared to PTCDA adsorbed on the similar $PbAg_2$ surface alloy where the formation of local σ-bonds between PTCDA and the Pb atoms results in a vertical relaxation of the Pb atoms coinciding with a strong modification of the surface alloy band structure. From this comparison, it can be concluded that adsorption-induced modifications of the structural and electronic properties of the surface alloy crucially depend on the presence or absence of σ-bonds between the molecular adsorbates and the surface alloy. The most obvious difference between both adsorbate systems is the significantly larger intrinsic vertical buckling of the clean alloy atoms for the $PbAg_2$ ($\Delta z_{\mathrm{Pb}}^{\mathrm{clean}} = 0.42 \pm 0.02$ Å) compared to the $SnAg_2$ surface alloy ($\Delta z_{\mathrm{Sn}}^{\mathrm{clean}} = 0.19 \pm 0.01$ Å). These different vertical positions of the alloy atoms result in different normalized bonding distances with the oxygen atoms of PTCDA. These, in turn, are eventually responsible for the formation of local σ-bonds at the PTCDA-surface alloy interface. While the vertical position of the alloy atoms can explain the different bonding of PTCDA to Sn- and Pb-based surface alloys on the Ag(111) surface, it cannot explain the recent findings of Cottin *et al.* [61] for PTCDA on the $BiAg_2$ surface alloy. They observed no modification of the $BiAg_2$ surface band structure although the vertical buckling of the Bi atoms of $\Delta z_{\mathrm{Bi}} = 0.65 \pm 0.10$ Å [30] even exceeds the one of Pb. The difference between Bi- and Pb-based

alloys can be attributed to the different occupation of their hybrid surface state with p_z character. While the p_z hybrid surface states of the bare $SnAg_2$ [48] and the $PbAg_2$ [32] surface alloy are only partially occupied, the Bi-Ag p_z hybrid surface state is completely filled [33] due to one additional valence electron of Bi compared to Sn and Pb [62]. This different population prevents the formation of σ-bonds between PTCDA and the $BiAg_2$ surface alloy atoms, which requires an effective charge transfer between the oxygen groups of PTCDA and the unoccupied (surface) states of the surface alloy [59]. In contrast, such a charge transfer is, in general, possible for surface alloys with partially occupied surface states such as the $SnAg_2$ and the $PbAg_2$ surface alloys, and can hence results in the formation of local σ-bonds for these surfaces.

Therefore, we can propose three empiric rules that define the necessary requirements of the formation of local σ-bonds between molecular complexes and surface alloy atoms: the existence of (i) functional and reactive molecular groups; (ii) only partially occupied hybrid surface states with p_z character; and (iii) a sufficient intrinsic vertical relaxation of the surface alloy atoms. These empiric rules represent the foundation for band structure engineering of surface alloys by the formation of tailored molecule-alloy surface bonds.

V. SUMMARY

In this work, we investigated the structural and electronic properties of the interface formed between PTCDA and the $SnAg_2$ surface alloy. The $SnAg_2$ surface alloy exhibits the well-known $(\sqrt{3}\times\sqrt{3})R30^\circ$ superstructure and a small but significant vertical relaxation of the Sn surface alloy atoms of 0.19 ± 0.02 Å with respect to the plane of the Ag surface atoms. The adsorption of PTCDA on the Sn-Ag surface alloy does not affect the structural (vertical position of the Sn atoms) and electronic properties (surface band structure) of the $SnAg_2$ surface alloy. This finding is in contrast to the behavior of PTCDA on a $PbAg_2$ surface alloy for which the molecular adsorption modifies both the surface band structure and the vertical relaxation of the Pb alloy atoms. This apparent contradiction could be resolved by the investigation of the vertical bonding distances and the charge redistribution at the interfaces. PTCDA adsorbs in a completely flat adsorption geometry on the $SnAg_2$ surface alloy without any structural indications for the formation of local σ-like bonds to the surface. In addition, no signs of interfacial charge transfer were observed. All these findings point to the mere physisorption of PTCDA/$SnAg_2$, and not to a chemical interaction with σ-like bonds as it was observed for the bare and the Pb-alloyed Ag(111) surfaces. In conjunction with previous findings for PTCDA on different surface alloys [36,50,61], we propose three empiric rules that define the necessities for the modification of surface alloys by σ-like bonding with molecular adsorbates: (i) functional and reactive molecular groups; (ii) only partially occupied hybrid surface states with p_z character; and (iii) a sufficient vertical relaxation of the surface alloy atoms. In this way, our work has uncovered the necessary ingredients for engineering the surface band structure of binary metallic surfaces and adsorbate systems by the formation of tailored molecule-surface bonds.

ACKNOWLEDGMENTS

The research leading to these results was funded by the Deutsche Forschungsgemeinschaft (DFG, German Research Foundation) – TRR 173 – 268565370 (project B05). M.F. and C.K also acknowledge financial support from the DFG via SFB 1083, B.S. from the Graduate School of Excellence Mainz (Excellence initiative DFG/GSC 266). L.L.K. thankfully acknowledges financial support from the Carl Zeiss Stiftung. M.C. acknowledges funding from the European Research Council (ERC) under the European Union's Horizon 2020 research and innovation programme (Grant Agreement No. 725767-hyControl). Moreover, we thank Diamond Light Source for access to beamline I09 (through proposal SI13773-1). We are very grateful for the support by the beamline staff during the experiment, in particular by P. K. Thakur, D. A. Duncan, T.-L. Lee, and D. McCue.

[1] F. Gutmann, L. E. Lyons, and H. Keyzer, *Organic Semiconductors* (Wiley, New York, 1967).
[2] H. Spanggaard and F. C. Krebs, Sol. Energy Mater. Sol. Cells **83**, 125 (2004).
[3] H. Ishii, K. Sugiyama, E. Ito, and K. Seki, Adv. Mater. **11**, 605 (1999).
[4] M. Schwarze, W. Tress, B. Beyer, F. Gao, R. Scholz, C. Poelking, K. Ortstein, A. A. Günther, D. Kasemann, D. Andrienko, and K. Leo, Science **352**, 1446 (2016).
[5] H. Xu, R. Chen, Q. Sun, W. Lai, Q. Su, W. Huang, and X. Liu, Chem. Soc. Rev. **43**, 3259 (2014).
[6] F. Tautz, Prog. Surf. Sci. **82**, 479 (2007).
[7] K. Seki, N. Hayashi, H. Oji, E. Ito, Y. Ouchi, and H. Ishii, Thin Solid Films **393**, 298 (2001).
[8] O. T. Hofmann, V. Atalla, N. Moll, P. Rinke, and M. Scheffler, New J. Phys. **15**, 123028 (2013).
[9] F. A. Ma'Mari, T. Moorsom, G. Teobaldi, W. Deacon, T. Prokscha, H. Luetkens, S. Lee, G. E. Sterbinsky, D. A. Arena, D. A. MacLaren, M. Flokstra, M. Ali, M. C. Wheeler, G. Burnell, B. J. Hickey, and O. Cespedes, Nature **524**, 69 (2015).
[10] X.-Y. Zhu, Surf. Sci. Rep. **56**, 1 (2004).
[11] C. H. Schwalb, S. Sachs, M. Marks, A. Schöll, F. Reinert, E. Umbach, and U. Höfer, Phys. Rev. Lett. **101**, 146801 (2008).
[12] M. Marks, N. L. Zaitsev, B. Schmidt, C. H. Schwalb, A. Schöll, I. A. Nechaev, P. M. Echenique, E. V. Chulkov, and U. Höfer, Phys. Rev. B **84**, 081301(R) (2011).
[13] S. Duhm, A. Gerlach, I. Salzmann, B. Bröker, R. Johnson, F. Schreiber, and N. Koch, Org. Electron. **9**, 111 (2008).
[14] I. Kröger, B. Stadtmüller, C. Stadler, J. Ziroff, M. Kochler, A. Stahl, F. Pollinger, T.-L. Lee, J. Zegenhagen, F. Reinert, and C. Kumpf, New J. Phys. **12**, 083038 (2010).
[15] Y. Zou, L. Kilian, A. Schöll, T. Schmidt, R. Fink, and E. Umbach, Surf. Sci. **600**, 1240 (2006).

[16] N. Koch, J. Phys.: Condens. Matter **20**, 184008 (2008).
[17] H. Ishii and K. Seki, IEEE Trans. Electron. Devices **44**, 1295 (1997).
[18] S. Lach, A. Altenhof, K. Tarafder, F. Schmitt, M. E. Ali, M. Vogel, J. Sauther, P. M. Oppeneer, and C. Ziegler, Adv. Funct. Mater. **22**, 989 (2012).
[19] S. Shi, Z. Sun, A. Bedoya-Pinto, P. Graziosi, X. Li, X. Liu, L. Hueso, V. A. Dediu, Y. Luo, and M. Fahlman, Adv. Functi. Mater. **24**, 4812 (2014).
[20] M. Cinchetti, V. A. Dediu, and L. E. Hueso, Nat. Mater. **16**, 507 (2017).
[21] B. Stadtmüller, D. Lüftner, M. Willenbockel, E. M. Reinisch, T. Sueyoshi, G. Koller, S. Soubatch, M. G. Ramsey, P. Puschnig, F. S. Tautz, and C. Kumpf, Nat. Commun. **5**, 3685 (2014).
[22] M. Häming, M. Greif, C. Sauer, A. Schöll, and F. Reinert, Phys. Rev. B **82**, 235432 (2010).
[23] O. R. Evans and W. Lin, Acc. Chem. Res. **35**, 511 (2002).
[24] E. Goiri, P. Borghetti, A. El-Sayed, J. E. Ortega, and D. G. de Oteyza, Adv. Mater. **28**, 1340 (2016).
[25] M. Cinchetti, S. Neuschwander, A. Fischer, A. Ruffing, S. Mathias, J.-P. Wüstenberg, and M. Aeschlimann, Phys. Rev. Lett. **104**, 217602 (2010).
[26] H. Ding and Y. Gao, Org. Electron. **11**, 1786 (2010).
[27] K. Akaike, A. Onishi, Y. Wakayama, and K. Kanai, J. Phys. Chem. C **123**, 12242 (2019).
[28] A. Haags, L. A. Rochford, J. Felter, P. J. Blowey, D. A. Duncan, D. P. Woodruff, and C. Kumpf, New J. Phys. **22**, 063028 (2020).
[29] P. J. Blowey, B. Sohail, L. A. Rochford, T. Lafosse, D. A. Duncan, P. T. P. Ryan, D. A. Warr, T.-L. Lee, G. Costantini, R. J. Maurer, and D. P. Woodruff, ACS Nano **14**, 7475 (2020).
[30] I. Gierz, B. Stadtmüller, J. Vuorinen, M. Lindroos, F. Meier, J. H. Dil, K. Kern, and C. R. Ast, Phys. Rev. B **81**, 245430 (2010).
[31] H. Bentmann, F. Forster, G. Bihlmayer, E. V. Chulkov, L. Moreschini, M. Grioni, and F. Reinert, Europhys. Lett. **87**, 37003 (2009).
[32] D. Pacilé, C. R. Ast, M. Papagno, C. Da Silva, L. Moreschini, M. Falub, A. P. Seitsonen, and M. Grioni, Phys. Rev. B **73**, 245429 (2006).
[33] C. R. Ast, J. Henk, A. Ernst, L. Moreschini, M. C. Falub, D. Pacilé, P. Bruno, K. Kern, and M. Grioni, Phys. Rev. Lett. **98**, 186807 (2007).
[34] L. Moreschini, A. Bendounan, I. Gierz, C. R. Ast, H. Mirhosseini, H. Höchst, K. Kern, J. Henk, A. Ernst, S. Ostanin, F. Reinert, and M. Grioni, Phys. Rev. B **79**, 075424 (2009).
[35] M. Ormaza, L. Fernandez, M. Ilyn, A. Magana, B. Xu, M. J. Verstraete, M. Gastaldo, M. A. Valbuena, P. Gargiani, A. Mugarza, A. Ayuela, L. Vitali, M. Blanco-Rey, F. Schiller, and J. E. Ortega, Nano Lett. **16**, 4230 (2016).
[36] B. Stadtmüller, J. Seidel, N. Haag, L. Grad, C. Tusche, G. van Straaten, M. Franke, J. Kirschner, C. Kumpf, M. Cinchetti, and M. Aeschlimann, Phys. Rev. Lett. **117**, 096805 (2016).
[37] L. Kilian, E. Umbach, and M. Sokolowski, Surf. Sci. **573**, 359 (2004).
[38] B. Kömker, M. Escher, D. Funnemann, D. Hartung, H. Engelhard, and J. Kirschner, Rev. Sci. Instrum. **79**, 053702 (2008).
[39] B. Stadtmüller, L. Grad, J. Seidel, F. Haag, N. Haag, M. Cinchetti, and M. Aeschlimann, J. Phys.: Condens. Matter **31**, 134005 (2019).
[40] T.-L. Lee and D. A. Duncan, Synchrotron Radiat. News **31**, 16 (2018).
[41] D. Woodruff, Prog. Surf. Sci. **57**, 1 (1998).
[42] D. P. Woodruff, Rep. Prog. Phys. **68**, 743 (2005).
[43] J. Zegenhagen, Surf. Sci. Rep. **18**, 202 (1993).
[44] D. Woodruff, Nucl. Instrum. Methods Phys. Res. Sect. A **547**, 187 (2005).
[45] F. Schreiber, K. Ritley, I. Vartanyants, H. Dosch, J. Zegenhagen, and B. Cowie, Surf. Sci. **486**, L519 (2001).
[46] I. Vartanyants, T.-L. Lee, S. Thiess, and J. Zegenhagen, Nucl. Instrum. Methods Phys. Res. Sect. A **547**, 196 (2005).
[47] G. van Straaten, M. Franke, F. C. Bocquet, F. S. Tautz, and C. Kumpf, J. Electron. Spectros. Relat. Phenom. **222**, 106 (2018).
[48] J. R. Osiecki and R. I. G. Uhrberg, Phys. Rev. B **87**, 075441 (2013).
[49] K. Glöckler, C. Seidel, A. Soukopp, M. Sokolowski, E. Umbach, M. Böhringer, R. Berndt, and W. D. Schneider, Surf. Sci. **405**, 1 (1998).
[50] B. Stadtmüller, N. Haag, J. Seidel, G. van Straaten, M. Franke, C. Kumpf, M. Cinchetti, and M. Aeschlimann, Phys. Rev. B **94**, 235436 (2016).
[51] A. Schöll, Y. Zou, M. Jung, T. Schmidt, R. Fink, and E. Umbach, J. Chem. Phys. **121**, 10260 (2004).
[52] A. Hauschild, R. Temirov, S. Soubatch, O. Bauer, A. Schöll, B. C. C. Cowie, T.-L. Lee, F. S. Tautz, and M. Sokolowski, Phys. Rev. B **81**, 125432 (2010).
[53] G. Mercurio, O. Bauer, M. Willenbockel, N. Fairley, W. Reckien, C. H. Schmitz, B. Fiedler, S. Soubatch, T. Bredow, M. Sokolowski, and F. S. Tautz, Phys. Rev. B **87**, 045421 (2013).
[54] G. Mercurio, Ph.D. thesis, RWTH Aachen, 2012.
[55] F. Bocquet, G. Mercurio, M. Franke, G. van Straaten, S. Weiß, S. Soubatch, C. Kumpf, and F. Tautz, Comput. Phys. Commun. **235**, 502 (2019).
[56] T. is a XSW data analysis simulation program written by F. C. Bocquet, G. Mercurio, and M. F. C. can be obtained from f.posseik@fz juelich.de.
[57] S. Alvarez, Dalton Trans. **42**, 8617 (2013).
[58] O. Bauer, G. Mercurio, M. Willenbockel, W. Reckien, C. Heinrich Schmitz, B. Fiedler, S. Soubatch, T. Bredow, F. S. Tautz, and M. Sokolowski, Phys. Rev. B **86**, 235431 (2012).
[59] L. Romaner, D. Nabok, P. Puschnig, E. Zojer, and C. Ambrosch-Draxl, New J. Phys. **11**, 053010 (2009).
[60] B. Stadtmüller, M. Willenbockel, E. M. Reinisch, T. Ules, F. C. Bocquet, S. Soubatch, P. Puschnig, G. Koller, M. G. Ramsey, F. S. Tautz, and C. Kumpf, Europhys. Lett. **100**, 26008 (2012).
[61] M. C. Cottin, J. Lobo-Checa, J. Schaffert, C. A. Bobisch, R. Möller, J. E. Ortega, and A. L. Walter, New J. Phys. **16**, 045002 (2014).
[62] H. Mirhosseini, A. Ernst, S. Ostanin, and J. Henk, J. Phys.: Condens. Matter **22**, 385501 (2010).